HHS Public Access
Author manuscript
Cancer Res. Author manuscript; available in PMC 2022 December 06.

Elimination of radiation-induced senescence in the brain tumor microenvironment attenuates glioblastoma recurrence

Eliot Fletcher-Sananikone[1,#], **Suman Kanji**[2,#], **Nozomi Tomimatsu**[2], **Luis Fernando Macedo Di Cristofaro**[3], **Rahul K. Kollipara**[4], **Debabrata Saha**[1], **John R. Floyd**[2], **Patrick Sung**[5], **Robert Hromas**[6], **Terry C. Burns**[7], **Ralf Kittler**[4], **Amyn A. Habib**[8,9], **Bipasha Mukherjee**[2], **Sandeep Burma**[2,4,*]

[1]Department of Radiation Oncology, University of Texas Southwestern Medical Center, Dallas, Texas.

[2]Department of Neurosurgery, University of Texas Health, San Antonio, Texas.

[3]School of Pharmaceutical Sciences, São Paulo State University (UNESP), Araraquara, Brazil.

[4]Eugene McDermott Center for Human Growth and Development, University of Texas Southwestern Medical Center, Dallas, Texas.

[5]Department of Biochemistry and Structural Biology, University of Texas Health, San Antonio, Texas.

[6]Department of Medicine, University of Texas Health, San Antonio, Texas.

[7]Department of Neurologic Surgery, Mayo Clinic, Rochester, Minnesota.

[8]Department of Neurology, University of Texas Southwestern Medical Center, Dallas, Texas.

[9]Veterans Affairs North Texas Health Care System, Dallas, Texas.

Abstract

Glioblastomas (GBM) are routinely treated with ionizing radiation (IR) but inevitably recur and develop therapy resistance. During treatment, the tissue surrounding tumors is also irradiated. IR potently induces senescence, and senescent stromal cells can promote the growth of neighboring tumor cells by secreting factors that create a senescence-associated secretory phenotype (SASP). Here, we carried out transcriptomic and tumorigenicity analyses in irradiated mouse brains to elucidate how radiation-induced senescence of non-neoplastic brain cells promotes tumor growth. Following cranial irradiation, widespread senescence in the brain occurred, with the astrocytic population being particularly susceptible. Irradiated brains showed an altered transcriptomic profile characterized by upregulation of CDKN1A (p21), a key enforcer of senescence, and several SASP factors including HGF, the ligand of the receptor tyrosine kinase (RTK) Met. Pre-irradiation of mouse brains increased Met-driven growth and invasiveness of orthotopically

*To whom correspondence should be addressed: Department of Neurosurgery, Department of Biochemistry and Structural Biology, University of Texas Health Science Center at San Antonio, 7703 Floyd Curl Drive, MC7843, San Antonio, TX 78229, USA. Phone: 210-450-8604; Fax: 210-567-6066 burma@uthscsa.edu.
#These authors contributed equally

implanted glioma cells. Importantly, irradiated p21−/− mouse brains did not exhibit senescence and consequently failed to promote tumor growth. Senescent astrocytes secreted HGF to activate Met in glioma cells and promote their migration and invasion in vitro, which could be blocked by HGF-neutralizing antibodies or the Met inhibitor crizotinib. Crizotinib also slowed the growth of glioma cells implanted in pre-irradiated brains. Treatment with the senolytic drug ABT-263 (navitoclax) selectively killed senescent astrocytes in vivo, significantly attenuating growth of glioma cells implanted in pre-irradiated brains. These results indicate that SASP factors in the irradiated tumor microenvironment drive GBM growth via RTK activation, underscoring the potential utility of adjuvant senolytic therapy for preventing GBM recurrence after radiotherapy.

Keywords

glioblastoma; ionizing radiation; tumor recurrence; tumor microenvironment; senescence; senolytic therapy

Introduction

Glioblastomas (GBM) are lethal brain tumors that are currently treated with high doses of ionizing radiation (IR). However, tumor relapse invariably occurs after radiotherapy, and the recurrent tumor is almost always refractory to further treatment (1). The standard-of-care for GBM comprises maximal safe resection followed by up to 60 Gy of fractionated IR with concurrent and adjuvant temozolomide (TMZ) (2). IR remains the mainstay of GBM therapy. Unfortunately, GBMs recur in the majority of patients after a relatively short period of time, with median progression-free survival ranging from 5.5 to 13 months (2). Despite the initial response of the tumor to IR, recurrence of GBM after radiotherapy is problematic as the recurrent tumor is more invasive (3) and therapy resistant (1). Recently published guidelines list repeat surgery (Re-S) and repeat radiation therapy (Re-RT) as options to treat recurrent GBM, but these and other strategies have limited efficacy (4), and therefore approaches to mitigate recurrence are an unmet need in GBM therapy.

Therapeutic strategies to delay tumor recurrence and to effectively treat recurrent tumors can only come from a mechanistic understanding of why GBM recurrence occurs after radiotherapy. Conventional radiation treatment volumes for GBM include a 2-3 cm margin around the tumor, and a majority of recurrences occur at or near this margin (5). Presumably, residual GBM cells in the margin evolve under therapeutic pressure resulting in recurrent tumors that are more therapy resistant (6). In addition to its effects on tumor cells, the high doses of radiation used for GBM therapy may also induce changes in the tumor microenvironment to help drive tumor recurrence. We hypothesized that radiotherapy of GBM induces senescence of non-neoplastic brain cells in the tumor microenvironment which promotes tumor recurrence, and also renders the recurrent tumor refractory to further therapy.

Cellular senescence is a state of persistent cell cycle arrest triggered by irreparable DNA damage, oxidative stress, telomere shortening, and oncogene activation. Senescence involves activation of the p53-p21 or p16^{Ink4a}-Rb tumor suppressor pathways, and prevents the further expansion of pre-malignant cells (7). However, recent research has revealed a

dangerous, pro-tumorigenic feature of senescence. Senescent cells secrete growth factors, interleukins, extracellular matrix (ECM) components, and ECM-modifying metalloproteases which together create a tumor-promoting senescence-associated secretory phenotype (SASP) (8,9). IR, which is commonly used for cancer therapy, is a potent inducer of senescence (8). Importantly, senescence of stromal cells has been shown to promote the growth of neighboring tumor cells via the SASP for cancers of the breast, lung, liver, and skin (10-19). Interestingly, certain cell types of the brain, especially astrocytes, are prone to senescence (20,21), and SASP in the brain contributes to age-related or toxin-induced neurodegeneration (22-26). Such pathological effects of the SASP can be countered by novel senolytic drugs that selectively induce apoptosis in senescent cells while sparing non-senescent cells (27,28). The phenomenon of cellular senescence and SASP has not been extensively studied in the brain in the context of their tumor-promoting potential. Here, we report that IR-induced senescence of astrocytes in the brain leads to the secretion of SASP factors that promote the growth and invasiveness of tumor cells in syngeneic mouse models of GBM, and that this can be mitigated with the senolytic drug ABT-263 (navitoclax). Our results open up the possibility of using adjuvant senolytic therapy to delay GBM recurrence, and to render the recurrent tumor responsive to additional treatment options.

Materials and Methods

Animal studies

C57BL/6J, FVB/NJ, BALB/cJ, and B6.129S6(Cg)-$Cdkn1a^{tm1Led}$/J (p21−/−) (29) mice (6-8 weeks in age) were purchased from Jackson Laboratories. FVB/NJ-C57BL/6J mixed background mice are maintained in house and have been described before (30). Mice were anesthetized using isoflurane and mounted on an acrylic bed equipped with a nose cone in prone position. Mice were cranially irradiated AP (anterior-posterior) with an X-ray device (X-RAD 320, Precision X-ray; 250 kV, 15 mA, 1.65 mm Al filter, at 5 cm) fitted with a specifically designed collimator providing a 10.08 mm-diameter field size iso-dose exposure while avoiding radiation exposure to the oropharynx as much as possible. The dose rate was 19.468 Gy/min, which was calibrated using a PTW 31010 ionization chamber and a PTW UnidosE electrometer (PTW North America Corporation) in accordance with the AAPM TG-61 protocol. The radiation dose was limited to 10 Gy as direct tongue irradiation with higher doses has been reported to cause oral mucositis in C57BL/6J mice (31). Control mice were anesthetized and sham irradiated. Mice were monitored periodically for weight loss and other symptoms of mucositis. For intra-cranial stereotactic injections, 2,500 luciferase-tagged GL261 or CT2A cells (32), or 50,000 NS2262 cells (30) were suspended in PBS (2μl) and delivered into the right corpus striatum of the brains of C57BL/6J, FVB/NJ-C57BL/6J, or p21−/− mice irradiated 30 days prior, as described previously (33). Tumor development was monitored by bioluminescence imaging. For senolytic studies, mice were treated with ABT-263 (50 mg/kg; Selleck Chem) in corn oil by daily oral gavage for 25 days or with vehicle alone as control, five days after cranial irradiation with 10 Gy, following which they were injected with GL261 or CT2A cells for tumor studies. For Met inhibition studies, 2,500 luciferase-tagged GL261 cells were injected intra-cranially in C57BL/6J mice 30 days after cranial irradiation with 10 Gy. Seven days after tumor cell implantation, crizotinib (50 mg/kg; Selleck Chem), dissolved in vehicle composed of 60%

Lipoid LLC Phosal 50PG (Thermo Fisher, Cat. No. NC0130871), 30% PEG 400 (Thermo Fisher) and 10% ethanol, was administered every alternate day by oral gavage for a total of 10 doses. Mice were sacrificed at the end of the experimental period or when they became moribund due to their tumor burden. Mice were perfused with 1X PBS followed by 4% PFA (paraformaldehyde; Sigma-Aldrich). Brains were dissected out, post-fixed by immersion in 4% PFA, and either embedded in paraffin or processed for cryosectioning. All animal studies were performed under protocols approved by the Institutional Animal Care and Use Committee of UT Health San Antonio and UT Southwestern Medical Center.

Noninvasive cranial bioluminescence imaging

Bioluminescence images of tumor-bearing mice were obtained using the IVIS Lumina System (Xenogen Corp.) coupled to Living Image data acquisition software (Xenogen Corp.), as described before (33). During imaging, mice were anaesthetized with isoflurane (Baxter International Inc.), and a solution of D-luciferin (180 mg/kg in PBS; Gold Biotechnology) was administered subcutaneously in the abdominal region. Images were acquired at 10 minutes post-luciferin administration and peak luminescence signals were recorded. The BLI signals emanating from the tumors were quantified by measuring photon flux within the region of interest (ROI) using the Living Image software package.

Histology and histopathology

Brains were fixed in 4% PFA (Sigma-Aldrich), embedded in paraffin, and sections were cut at 5 μm thickness. Sections were stained with hematoxylin and eosin (H&E, Vector Laboratories), as described previously (30). Slides were digitally scanned using Hamamatsu NanoZoomer 2.0-HT. Histopathological analysis was performed on NDP.View2. Invasion index was calculated as $1/(4\pi \times \text{area} / \text{perimeter}^2)$ of the tumor (34). Terminal deoxynucleotidyl transferase-mediated dUTP nick end labeling (TUNEL) staining was performed on paraffin sections using the TUNEL Assay Kit - HRP-DAB (Abcam, Cat. No. 206386), as per manufacturer's directions. TUNEL labeling was quantified by counting the number of TUNEL-positive cells per visual field (40X).

Immunofluorescence staining

Formalin-fixed, paraffin-embedded brain sections were deparaffinized, re-hydrated, and stained using standard protocols, as described previously (30). Briefly, antigen retrieval was performed at 98°C for 20 min, at 15psi, in 10mM citrate buffer (pH 6) in a commercial pressure cooker for all antibodies. Tissue sections were blocked in Goat Serum (Vector Laboratories) for 30 minutes in TBS prior to overnight incubation in primary antibody, following which sections were incubated with Alexa 488/568- conjugated secondary antibodies (Invitrogen) for 1 hour prior to mounting in Vectashield with 4',6-diamidino-2-phenylindole (DAPI; Vector Laboratories). The following primary antibodies were used: p21 (Abcam, Cat. No. 1888224), Lamin B1 (Abcam, Cat. No. 16048), pMET Tyr1234/1235 (Cell Signaling, Cat. No. 3077S), GFAP (Biocare, Cat. No. CP040A). Immunofluorescence images were acquired with a Zeiss Axio Imager 2 motorized inverted microscope with an Axiocam camera and ZEN imaging software (Carl Zeiss). The percentage of p21+/GFAP+, Lamin B1+/GFAP+, or Lamin B1+/DAPI+ cells was calculated by counting the number of

GFAP– or DAPI-positive cells that also co-stained with p21 or Lamin B1 per visual field (40X).

Senescence-associated β-galactosidase staining

In vitro staining of cells was carried out using the Senescence β-Galactosidase Staining Kit (Cell Signaling, Cat. No. 9860) as per the manufacturer's protocol. For *in vivo* staining, brains were harvested after perfusing mice with PBS and fixed in 4% paraformaldehyde overnight at 4°C and then equilibrated in 30% sucrose for 24 hours at 4 °C. Brains were embedded in OCT compound (Fisher), and 5 μm-thick frozen sections were cut. Sections were mounted onto a slide and encircled using a hydrophobic pap pen. Slides were stained with Senescence β-Galactosidase Staining Kit (Cell Signaling, Cat. No. 9860) overnight as per the manufacturer's protocol. Slides were washed with ddH$_2$O, counterstained with DAPI (Thermo-Fisher, Cat. No. D1306), and mounted in a 50% Glycerol solution. Images of the primary somatosensory area were captured on BZ-X Series All-in-one Fluorescence Microscope. The number of cells positive for senescence-associated β-Galactosidase activity per visual field (40X) were counted in triplicate.

Astrocyte isolation and cell culture

Primary mouse astrocytes were isolated from 1-2 days old C57BL/6J pups as per published protocols (35). Briefly, brains were dissected out from 4 pups from the same litter and pooled for each culture. The brains were mechanically dissociated by pipetting and enzymatic digestion in 2.5% trypsin, and then plated in a T75 flask. Media was changed after 2 days, and after 7-8 days, and once cells were adherent and confluent, cell debris and non-astrocytic cell types were removed by mechanical shaking. The homogeneity of the final astrocytic population obtained by this method was verified by immunofluorescent staining for the astrocytic marker GFAP (35). Primary astrocytes, and GL261 and CT2A cells (32) were cultured in DMEM media supplemented with 10% Fetal Bovine Serum and penicillin/streptomycin (100 μg/ml) in a humidified 37°C incubator with 5% CO$_2$. NS2262 neurosphere cultures were maintained in serum-free DMEM/F-12 1:1 media (Life Technologies) supplemented with B27 without Vitamin A (Life Technologies), 10 ng/mL EGF (PeproTech), and 10 ng/mL basic FGF (PeproTech), as described earlier (30). All cells were mycoplasma free. Early passage cells were used for experiments.

Protein extraction and western blotting

Brains isolated from mock-irradiated or irradiated C57BL/6J mice were homogenized in NP-40 lysis buffer (10 mM Tris–HCl, pH 8.0, 150 mM NaCl, 1% NP-40, and protease and phosphatase inhibitor cocktails). Extracts were clarified by centrifugation at 16,000 g at 4 °C and the supernatant was collected and processed for western blotting. Cells in culture were washed with cold PBS, collected using a cell scraper, and centrifuged at 2000 *g* for 5 min. The pellets were lysed with NP-40 lysis buffer, followed by sonication and centrifugation at 16,000 *g* at 4°C. The supernatant was collected, and protein concentration was measured by the Bradford assay (Bio-Rad) prior to preparation of samples for SDS-PAGE and western blotting. Antibodies used for western blotting are as follows: HGF (Abcam, Cat. No. 83760), p21 (Abcam, Cat. No. 1888224), β-Actin (Santa Cruz, Cat. No. 47778), Lamin B1 (Abcam, Cat. No. 16048), phospho-Met Tyr1234/1235 (Cell Signaling, Cat. No. 3077S), Met (Cell

Signaling, Cat. No. 8198), GAPDH (Cell Signaling, Cat. No. 5174), and HRP-conjugated secondary antibodies (Bio-Rad).

Migration assay

Primary mouse astrocytes were seeded into 48 well plates (Thermo Fisher) at 50,000 cells per well and allowed to recover for 24 hours. The astrocytes were then irradiated with 10 Gy of X-rays. After 10 days incubation, 10,000 GL261 or CT2A cells were seeded in cell culture inserts (Thermo Fisher) with 8 μm pore size, and the inserts were placed in wells with mock-irradiated or irradiated astrocytes. Cells were allowed to incubate for 24 hours. The cell culture inserts were removed, and the upper surface cleansed with a cotton swab. Inserts were washed in PBS, fixed in 4% paraformaldehyde for 15 minutes, and stained with Alexa Fluor 488 Phalloidin (Thermo Fisher, Cat. No. A12379) in PBS overnight. Cell culture insert membranes were removed per manufacturer's directions and mounted onto glass slides, counterstained with DAPI, and immunofluorescence images of the lower surface were acquired with a Zeiss Axio Imager 2 motorized inverted microscope with an Axiocam camera and ZEN imaging software (Carl Zeiss). The number of cells per visual field (40X) was quantified and normalized to the control to obtain relative cell migration. Crizotinib (Millipore-Sigma, Cat. No. PZ0191, 500 nM) or anti-mouse HGF antibody (R&D Systems, Cat. No. AF2207, 1μg/ml) were administered at the same time as when glioma cells were seeded. All experiments were performed in triplicate.

Enzyme-linked immunosorbent assay (ELISA)

Primary mouse astrocytes were seeded in T25s and either mock-irradiated or irradiated with 10 Gy of X-rays. Ten days after irradiation, conditioned media was collected from the cells and the levels of HGF measured using a mouse HGF DuoSet ELISA kit (R&D System, Cat no. DY2207), in accordance with the manufacturer's protocol. Assay plates were read at 450 nm with an Epoch microplate spectrophotometer (BioTek Instruments). Concentrations of the unknown samples were then calculated from the standard curve using slope and the intercept from the absorbance output.

RNA-Seq of brain tissues

Mice were perfused with PBS and brains were dissected out. Total RNA was extracted from dissected whole brains using TRIzol (Invitrogen) according to the manufacturer's instructions. RNA quantity was then determined using a Qubit fluorometer (Thermo Fisher), and RNA quality was analyzed with an RNA tape on the 4200 TapeStation (Agilent). TruSeq Stranded Total RNA Ribo-Zero kit (Illumina) was used to prepare sequencing libraries from 2 μg total RNA. Sequencing was performed on the NextSeq500 using 75 nucleotide single end SBS chemistry, with ~30-40 Million reads for each sample. Sequence reads were aligned to the mouse transcriptome using TopHat (36). The alignment was processed further using the Cufflinks package to quantify transcript levels and to identify differentially expressed genes (37). For visualization of Cufflinks analyses we used the CummeRbund package. The following cutoffs were used to select differentially expressed genes of interest: a minimum FPKM of >=1 and <= 5% FDR.

Quantitative reverse transcription PCR

Total RNA was extracted from cells in culture and purified using TRIzol (Invitrogen), according to the manufacturer's instructions. cDNA synthesis was performed using SuperScript™ III First-Strand Synthesis System (Invitrogen) following manufacturer's instructions. Quantitative PCR was performed to analyze gene expression using SYBR Green PCR master mix on Bio-Rad CFX96 with CFX Maestro Analysis Software (see Supplemental Table for primer sequences). All samples were amplified in triplicate. Measurements were standardized to *GAPDH* housekeeping gene. Expression data is presented as fold change using delta-delta Ct to measure statistical significance in the observed changes.

Statistical analysis

Statistical analyses were performed by using two-tailed Student's t-test or One Way Anova (for multiple comparisons) with GraphPad Prism (GraphPad 7 Software). Error bars represent S.D. when multiple visual fields were averaged to produce a single value for each animal which was then averaged again to represent the mean bar for the group in each graph. Error bars for IVIS imaging represent S.E.M when individual signal intensities (photons per sec) were averaged for each cohort. Statistical significance was defined as $P < 0.05$. Kaplan-Meier functions were used to illustrate survival profiles using Mantel-Cox test.

Data availability

Raw and processed RNA-seq data generated in this study are available at Gene Expression Omnibus under accession GSE184451.

Results

Pre-irradiation of the brain promotes GBM growth and aggressiveness.

In order to understand whether irradiation of non-neoplastic brain cells promotes GBM growth, we utilized a syngeneic mouse glioma model that constituted immunocompetent C57BL/6J mice implanted with luciferase-tagged GL261 mouse glioma cells (32). C57BL/6J mice were first mock-irradiated or cranially irradiated with a single dose of 10 Gy of X-rays. After 30 days, the mice were intra-cranially implanted with a limiting number (2,500) of GL261 cells, and tumor growth was monitored over a 30-day period (Fig. 1A). Irradiation of mouse brains prior to tumor cell implantation resulted in a striking increase in tumor growth rates as determined by recording and plotting BLI radiance over time (Fig. 1B,C). At 30 days post-implantation, the mice were sacrificed, and their brains harvested and sectioned for histopathological analyses. Pre-irradiated mouse brains harbored tumors that were larger compared to those in mock-irradiated brains, in concordance with the BLI data (Fig. 1D). Importantly, tumors growing in pre-irradiated brains were significantly more infiltrative, as quantified by measuring the tortuosity of the tumor border (34) (Fig. 1D,E). In order to understand how the observed differences in tumor growth and pathology affected long-term survival of tumor-bearing mice, we repeated the study and monitored mice until they became moribund. As is evident from the Kaplan-Meier plots, pre-irradiation of mouse brains significantly shortened the time to death after tumor cell implantation (Fig.

1F). In order to confirm that these results were not unique to the GL261 line, we repeated these experiments with a different syngeneic mouse glioma line - CT2A (32). We found that pre-irradiation of mouse brains resulted in a striking increase in CT2A tumor growth and invasiveness, similar to that observed with the GL261 cells (Supplemental Fig. 1A-C). Accordingly, pre-irradiated mice bearing CT2A tumors exhibited poorer survival compared to mock-irradiated mice (Supplemental Fig. 1D). As both GL261 and CT2A cells have the same genetic background (32), we wanted to validate our results using glioma cells with a different genetic background. We utilized a neurosphere line (NS2262), previously generated by us from a glioma arising in a mouse with a mixed FVB/NJ-C57BL/6J background (30). We found that pre-irradiation of the brains of FVB/NJ-C57BL/6J mice resulted in augmented growth of NS2262 cells implanted at 30 days post-IR, along with decreased survival of pre-irradiated tumor-bearing mice (Supplemental Fig. 1E,F). Taken together, these results indicate that IR engenders a pro-tumorigenic environment in the brain making it conducive to glioma growth, and promotes tumor invasiveness with a corresponding decrease in survival of tumor-bearing mice.

Ionizing radiation triggers senescence of astrocytes and induces the SASP in the brain.

We hypothesized that IR-induced senescence of non-neoplastic brain cells and the resulting SASP might drive the aggressive growth of glioma cells that we observed in pre-irradiated brains. A bona fide marker of senescence is the expression of senescence-associated β-galactosidase (SA-β-gal) activity (38). To determine whether IR induced a senescent phenotype in the brain, we carried out SA-β-gal staining of the brains of C57BL/6J mice that were mock irradiated or irradiated with 10 Gy of IR, and then allowed to recover for 30 days (Fig. 2A). We found significantly elevated SA-β-gal activity in the brains of irradiated mice (Fig. 2B,C). Astrocytes are one of the most abundant cell types in the brain (39), and have been shown in previous studies to be prone to senescence in response to IR or environmental toxins (20-23,26). We therefore co-stained mock-irradiated and irradiated brain sections for the astrocytic marker glial fibrillary acidic protein (GFAP) (40) and for two independent markers of senescence – increased expression of p21 (38) and loss of nuclear Lamin B1(41). Immunofluorescent co-staining showed that GFAP-positive cells co-stained with p21 in irradiated brains but not in mock-irradiated brains (Fig 2D,E). In concordance with the p21 results, GFAP-positive cells showed loss of nuclear Lamin B1 in irradiated but not in mock-irradiated brains (Fig. 2F,G). In order to confirm that IR-induced senescence was not unique to the C57BL/6J strain, we cranially irradiated mice with two different genetic backgrounds (BALB/cJ and FVB/NJ), and assessed nuclear Lamin B1 levels after 30 days; we found evidence of loss of Lamin B1 in these additional strains of mice (Supplemental Fig. 2A,B).

To determine whether IR induced the SASP in the brain, we carried out RNA-Seq analyses of RNA extracted from brain tissues of mice that were mock-irradiated or irradiated with 10 Gy of X-rays, at 30 days post-irradiation (Fig. 2H). The RNA-Seq data revealed an increase in the expression of a number of genes associated with the SASP (9,42,43) (Supplemental Fig. 2C). In light of our observations of senescent astrocytes in the irradiated brain (Fig. 2D-G), we wanted to evaluate if the astrocytic population contributed to the observed upregulation of SASP factors. We isolated primary astrocytes from C57BL6/J

pups, then mock-irradiated or irradiated these astrocytes with 10 Gy of X-rays, and assessed senescence after 10 days by SA-β-gal staining. We found that irradiated astrocytes showed significant levels of SA-β-gal-positivity, confirming our in vivo observations of radiation-induced senescence of astrocytes in the mouse brain (Fig. 2I,J). Next, we isolated mRNA from mock-irradiated or irradiated astrocytes and used qRT-PCR to validate the top 14 SASP-related genes whose expression was significantly increased in the irradiated brain (Supplemental Fig. 2D). We found enhanced expression of 13 of these genes in the senescent astrocytes (Fig. 2K). To assess the relevance of these genes to GBM development, we queried the TCGA database using cBioportal (44,45). Among these 13 genes, *HGF* was most commonly altered in GBM (Supplemental Fig. 2E). We next irradiated or mock-irradiated mouse brains with 10 Gy of IR and assessed HGF levels by western blotting at 30 days post-IR. We observed increased expression of HGF, as well as of p21, in the irradiated brain extracts, confirming results obtained by RNA-seq and qRT-PCR (Supplemental Fig. 2F-H). Taken together, these results indicate that IR triggers senescence in the brain and that senescent astrocytes contribute to the upregulation of SASP factors, notably HGF, in the irradiated brain.

Senescence and tumor promotion caused by ionizing radiation are p21-dependent.

The cyclin-dependent kinase (CDK) inhibitor p21 is a key enforcer of senescence in response to DNA damage (7). In light of the increased p21 expression in the irradiated brains (Fig. 2D,E; Supplemental Fig. 2F,H), we wanted to determine if senescence induced by IR was p21 dependent. To this end, we cranially irradiated p21+/+ and p21−/− mice (C57BL/6J background) (29) with 10 Gy of X-rays and assayed for senescence markers after 30 days. Unlike p21+/+ brains, p21−/− brains did not exhibit a significant increase in SA-β-gal activity (Fig. 3A,B) or decrease in nuclear Lamin B1 (Fig. 3C,D) after irradiation, indicating that IR-induced senescence is dependent on p21. Correspondingly, p21−/− astrocytes irradiated in vitro did not show a significant increase in HGF expression compared to their wild type counterparts (Supplemental Fig. 3A). Next, we cranially irradiated p21+/+ and p21−/− mice, and implanted GL261 cells after 30 days. Interestingly, pre-irradiation of the p21−/− mice did not affect tumor growth as assessed by BLI imaging in contrast to the accelerated tumor growth seen in pre-irradiated p21+/+ mice (Fig. 3E,F). We repeated this experiment with the CT2A glioma line, and found that pre-irradiation of p21−/− mice resulted in a much smaller increase in tumor growth compared to that seen in p21+/+ mice (Supplemental Fig. 3B). These results indicate that the accelerated brain tumor growth seen in pre-irradiated mouse brains is driven by p21-dependent senescence of cells in the tumor microenvironment.

Irradiated astrocytes promote migration of GBM cells in vitro via HGF secretion.

The SASP factor HGF (46) activates the MET receptor tyrosine kinase (RTK) which promotes the invasion of cancer cells and maintains a cancer stem cell (CSC) phenotype in GBM (47). The increased expression of HGF in senescent brains piqued our interest not only because the tumors growing in pre-irradiated brains were more invasive (Fig. 1D,E; Supplemental Fig. 1B,C), but also because we had previously observed that Met amplification was the most common genetic alteration in radiation-induced gliomas in mouse models (30,48). We therefore wondered whether secretion of HGF by senescent

astrocytes might activate MET in the tumor cells resulting in increased tumor growth and invasiveness. Upon immunofluorescence staining of GL261 tumor sections, we found that tumors in pre-irradiated brains stained intensely for phospho-Met (Tyr1234/1235), indicating robust Met activation, in contrast to tumors in mock-irradiated brains (Fig. 4A). To better understand the effect of senescent astrocytes on the behavior of glioma cells, we isolated primary astrocytes from C57BL6/J pups and mock-irradiated or irradiated them with 10 Gy to induce senescence. Induction of senescence at 10 days post-IR was confirmed by western blotting of astrocyte extracts for Lamin B1(Supplemental Fig. 4A). Next, we treated GL261 or CT2A cells with conditioned media from the senescent astrocytes. We saw activation of the Met RTK in the recipient cells as evaluated by western blotting for phospho-Met (Tyr1234/1235) indicating that the senescent astrocytes release the Met ligand – HGF – into the media (Supplemental Fig. 4B). The release of HGF by senescent astrocytes was confirmed by ELISA of conditioned media from astrocytes at 10 days post-IR (Supplemental Fig. 4C). Next, we used the Boyden Chamber assay to evaluate the effect of senescent astrocytes on the migration of glioma cells. We found that irradiated primary astrocytes (at day 10 post-IR) significantly promoted the migration of GL261 cells across the transwell membrane while mock-irradiated astroctyes had no such effect (Fig. 4B,C). Senescent astrocytes similarly promoted the migration of CT2A cells in a trans-well assay (Supplemental Fig. 4D,E). Senescent astrocytes also promoted the invasion of GL261 cells through Matrigel in a trans-well assay (Supplemental Fig. 4F,G). In light of these observations, we wanted to determine whether blocking the HGF-MET axis might attenuate migration of glioma cells driven by senescent astrocytes. We repeated the Boyden Chamber assay after adding either control IgG or HGF-neutralizing antibody to the culture medium. The addition of HGF-neutralizing antibody attenuated migration though the transwell membrane (Fig. 4D,E). Similarly, addition of the MET inhibitor crizotinib (49) to the GL261 culture medium lead to a decrease in cell migration (Fig. 4F,G). Next, we implanted GL261 cells in C57BL/6J mice 30 days after cranial irradiation with 10 Gy of X-rays. Seven days after tumor cell implantation, the mice were treated with 10 doses of crizotinib (50 mg/kg) given every other day or with vehicle alone as control. Treatment with crizotinib resulted in a modest attenuation of tumor growth and increased survival of tumor-bearing mice, indicating that MET activation contributes to the enhanced tumor growth seen in pre-irradiated mouse brains (Supplemental Fig. 4H,I). Finally, we wanted to validate the tumor-promoting effects of senescent astrocytes in an in vivo setting. We mixed mock-irradiated or irradiated (senescent) astrocytes with GL261 cells (5:1 ratio), and implanted the cells intra-cranially in C57BL/6J mice. Upon monitoring tumor growth by BLI imaging, we observed faster tumor growth when the GL261 cells were implanted together with senescent astrocytes relative to implantation with mock-irradiated astrocytes (Supplemental Fig. 4J). Taken together, these results indicate that the secretion of HGF by senescent astrocytes and consequent activation of Met promotes the migration and growth of glioma cells both in vitro and in vivo.

ABT-263 eliminates senescent cells *in vivo* resulting in delayed tumor growth in pre-irradiated brains.

In order to conclusively prove that senescence in the irradiated brain drives tumor growth, we sought to pharmacologically eliminate senescent cells prior to implantation of tumor

cells. A number of senolytic drugs are currently under investigation for their ability to specifically kill senescent cells without affecting proliferating and quiescent cells (27,28). However, in the context of the brain, a key clinical issue is a drug's ability to cross the blood-brain-barrier. We chose the senolytic compound ABT-263 (navitoclax) as it has been previously shown to clear senescent astrocytes in a mouse model Alzheimer's disease (26), and has been shown to cross the blood-brain-barrier in other studies (21,50). We irradiated C57BL6/J mice with 10 Gy of X-rays and allowed them to recover for 5 days. Then, mice were treated with either corn oil (hereafter designated as vehicle) or with 50 mg/kg ABT-263 in corn oil given daily for 25 days (Fig. 5A). We assessed irradiated brains after the treatment period by SA-β-gal staining. There were significantly fewer senescent cells in the brains of mice treated with ABT-263 compared to vehicle alone (Fig. 5B,C). We also observed a concomitant increase in TUNEL positivity in the mouse brains indicating clearance of senescent cells via induction of apoptosis (Fig. 5D,E). Given the observed elimination of senescent cells, we wanted to determine if we could use ABT-263 to ameliorate the pro-tumorigenic effects of IR on the brain. We therefore irradiated C57BL6/J mice with 10 Gy of X-rays, and allowed them to recover for 5 days before treating them with either vehicle or ABT-263 for 25 days. The mice were then intra-cranially injected with GL261 cells and monitored for tumor growth and survival. Tumor growth was significantly delayed (Fig. 5F), and survival was prolonged (Fig. 5G) in ABT-263-treated mice, confirming the critical role of senescent astrocytes in supporting glioma growth. Similar results were obtained with irradiated mice implanted with CT2A cells, with mice pre-treated with ABT-263 showing slower tumor growth and improved survival compared to vehicle-treated mice (Supplemental Fig. 5A,B). Interestingly, histopathological analyses revealed a remarkable increase in tumor necrosis in the ABT-263-treated mice as compared to the vehicle-treated mice (Fig. 5H) along with increased apoptosis (TUNEL positivity) in the non-necrotic areas of the tumor (Fig. 5I,J), though tumor invasiveness was not reduced significantly (Supplemental Fig. 5C). Taken together, these data indicate that elimination of senescent cells in the irradiated brain results in attenuated tumor growth and increased tumor cell death resulting in improved survival of ABT-263-treated mice.

Discussion

IR, in combination with TMZ, is the most effective therapeutic modality for the treatment of GBM, and will likely remain part of the standard-of-care for the foreseeable future. However, the inevitable recurrence of GBM after radiotherapy presents a unique problem as the recurrent tumor is usually very resistant to further therapeutic interventions (1). In order to delay tumor recurrence or to treat the recurrent tumor, it would be important to understand not only how radiation alters the tumor cell, but also its effects on the tumor microenvironment. A previous study had shown that radiotherapy of human brain tumors results in senescence in the non-tumor regions of the brain (20). This is not surprising as these tumors are treated with up to 60 Gy of IR, and the treatment volume includes a 2-3 cm margin of normal brain tissue surrounding the tumor (5). We therefore asked whether radiation-induced senescence in the GBM microenvironment might actually drive tumor recurrence via development of the SASP (8,9).

We found that IR triggered widespread senescence in the mouse brain, as verified by a number of markers including SA-β-gal- and p21-positivity, loss of nuclear Lamin B1, and upregulation of bona fide SASP genes (9,42). By co-immunostaining mouse brain sections for GFAP and senescence markers, we found that astrocytes in the mouse brain were particularly prone to senescence. This is congruent with previous studies showing that astrocytes comprised the bulk of senescent cells in irradiated human and mouse brains (20,21) and in the brains of patients with Alzheimer's disease (23). Our results are also in concord with other studies showing that astrocytic senescence contributes to radiation-, neurotoxin- or tau-induced neurodegeneration (20-23,26). While astrocytes are the most abundant cell type in the brain (39), microglia and endothelial cells have also been reported to undergo senescence in irradiated human brains albeit to a lesser extent than astrocytes (20), and the extent to which these cell types contribute to the SASP certainly warrants further investigation.

Interestingly, we found that senescent astrocytes in the irradiated mouse brain promoted the growth of murine glioma cells implanted 30 days after irradiation, resulting in tumors that were more invasive and lethal compared to those growing in mock-irradiated brains. These findings were supported by additional experiments showing that co-implantation of senescent astrocytes with glioma cells in mouse brains significantly promoted tumor growth. These findings are consistent with prior observations of aggressive growth of human glioma cells in cranially-irradiated nude mice (51). A number of studies have shown that senescence of stromal cells promotes the growth of neighboring tumor cells for a number of cancers via multiple mechanisms, including a) establishment of an immunosuppressive microenvironment (17), b) secretion of MMPs that alter the tumor microenvironment (12-14), c) secretion of ECM components (16), d) increased tumor vascularization via secretion of vascular endothelial growth factor (11), and e) direct mitogenic action on tumor cells via secretion of interleukins and growth factors like HGF (13,18,19). These studies led Judith Campisi and co-workers to propose that therapy-induced senescence (TIS) of stromal cells could promote cancer relapse, illustrating this concept in a mouse model of breast cancer treated with doxorubicin (8,10). Our study in mouse models of GBM shows that the concept of TIS-driven tumor recurrence is applicable to radiotherapy of brain tumors and perhaps other cancers that are treated with radiation.

The effect of senescent stromal cells on tumor growth has been attributed to the SASP, the exact composition of which appears to be dynamic and dependent upon the cell type, the senescence-triggering stimulus, and time elapsed after induction of senescence (7). Regardless of these dynamics, the tumor promoting effects of the SASP have been broadly attributed to growth factors, interleukins, MMPs, and ECM components (8,9). Our analyses of senescent mouse brains and senescent astrocyte cultures showed upregulation of a number of genes with well-understood tumor promoting effects, many of which code for bona fide SASP factors. Of these genes, we chose to focus on *HGF* because the tumors in pre-irradiated (senescent) brains exhibited increased tumor growth and invasiveness, phenotypes associated with activation of the HGF receptor Met (47,49). Moreover, of the top 13 SASP-related genes that we found to be significantly upregulated in both irradiated mouse brains and senescent astrocytes, *HGF* was the one seen to be most commonly altered in GBM upon querying the TCGA database. Indeed, HGF/MET are reported to be highly expressed

in GBM with their expression directly correlating with tumor grade (52). Furthermore, we had shown previously that Met is frequently amplified in radiation-induced GBMs in mouse models, indicating that secretion of HGF by senescent astrocytes might favor the selection of incipient GBM cells with Met amplification (30,48). The increased expression of HGF in irradiated brains, overexpression of HGF/MET in high grade gliomas, and Met amplification in radiation-induced GBM all indicate a critical role for HGF in radiation-driven GBM growth. In support of such a role for HGF in promoting GBM recurrence and invasiveness after radiation, we found that secretion of HGF by senescent astrocytes resulted in Met activation in tumor cells and promoted tumor cell migration and invasion in vitro, and that this could be blocked by HGF-neutralizing antibodies or the Met inhibitor crizotinib. Interestingly, paracrine secretion of HGF by cells of the tumor-reactive stroma has been shown to confer therapy resistance to tumor cells via MET activation in several cancer contexts (53,54), and promotion of tumor growth by senescent stromal fibroblasts has been attributed to HGF secretion in studies involving prostate and breast cancer cells (13,18). These studies clearly indicate that stromal cells secreting HGF can promote tumor growth, invasion and therapy resistance via MET activation, a situation analogous to HGF secretion by irradiated astrocytes in the context of brain tumors.

It is important to stress here that the secretion of HGF by senescent astrocytes would be only one mechanism of tumor promotion, and that other SASP factors must also drive tumor recurrence, invasion, and therapeutic resistance via alternate mechanisms. Hence, a therapeutic strategy involving only one such SASP-related pathway would, at best, be partially successful, as illustrated by the modest effects of the Met inhibitor crizotinib in our study. Instead, strategies involving the elimination of senescent cells from the tumor microenvironment might achieve higher therapeutic efficacy. The selective elimination of senescent cells has been made possible by intense research in this area over the last decade, leading to the discovery and validation of "senolytic" drugs and their testing in multiple ongoing clinical trials (27,28). Since senescent cells are highly resistant to apoptosis, targeting pro-survival pathways in these cells is currently the most common senolytic strategy. These approaches include targeting anti-apoptotic proteins, the effectiveness of which is illustrated by ABT-263 (navitoclax), a selective inhibitor of BCL-2 family members. ABT-263 can selectively induce apoptosis in a variety of cells undergoing senescence in response to IR, oncogene activation or replicative exhaustion (55). ABT-263 can also deplete senescent cells in vivo, rejuvenating the hematopoietic system in whole body irradiated mice (56), preventing age-related bone loss in mice (57), mitigating IR-induced pulmonary fibrosis (58), and attenuating bleomycin-induced dermal fibrosis (59). Though ABT-263 shows platelet toxicity, this can be ameliorated by appropriate dosing schedules and by the use of PROTAC technology (60). In this study, we chose to use ABT-263 as a tool to eliminate senescent cells in the irradiated mouse brain as it has been shown to cross the blood-brain-barrier and clear senescent astrocytes in vivo in multiple studies (21,26,50). We found that ABT-263, administered over 25 daily cycles after cranial irradiation, could eliminate senescent cells in the brain by triggering apoptosis in these cells. Clearance of senescent cells resulted in slower growth of glioma cells implanted after ABT-263 treatment and improved survival of tumor bearing mice. With improved

senotherapeutics in the pipeline, these results could inform future studies for the evaluation of senolytics as an adjuvant in GBM therapy.

It has been proposed that senolytics would be most effective if deployed as part of a two-step anticancer regimen – chemotherapy to induce senescence in tumor cells followed by senotherapy to eliminate senescent tumor cells (61). Such a "one-two punch" – radiation/TMZ followed by adjuvant senolytic therapy – could be beneficial for GBM treatment for more than one reason. While we find that radiation induces senescence in non-neoplastic brain cells, other studies have shown that both IR and TMZ induce senescence in GBM cells (62,63). Thus, adjuvant senolytic therapy would not only eliminate tumor-promoting senescent astrocytes in the microenvironment, but would also eliminate the fraction of GBM cells that have undergone senescence after radio-chemotherapy. The latter might be critically important because senescent tumor cells that eventually escape senescence acquire cancer stem cell properties and contribute aggressively to tumor relapse (64). It is important to point out here that while our study was focused on the induction of stromal senescence by IR, future studies are needed to understand the senescence-promoting effects of TMZ (alone or in combination with IR). Also, while the results from this study illustrate how senescent astrocytes in the tumor microenvironment influence GBM aggressiveness, future studies in pre-clinical models will be necessary to determine whether adjuvant senolytic therapy could be translated to the clinic to delay GBM recurrence and to render the recurrent tumor more responsive to further therapeutic interventions. An added benefit of senolytic therapy could be amelioration of neurodegeneration and cognitive deficits arising as a consequence of radiotherapy in brain tumor patients (65). Indeed, navitoclax was recently shown to ameliorate the loss of neurovascular coupling leading to cognitive preservation in a murine model of brain radiation (21). In sum, these results demonstrate that radiation-induced senescence in the tumor microenvironment drives GBM growth, and lay the foundation for future studies analyzing the utility of senolytics to prevent GBM recurrence after radiotherapy.

Supplementary Material

Refer to Web version on PubMed Central for supplementary material.

Acknowledgements

References

1. Osuka S, Van Meir EG. Overcoming therapeutic resistance in glioblastoma: the way forward. The Journal of clinical investigation 2017;127:415–26 [PubMed: 28145904]

2. Stupp R, Mason WP, van den Bent MJ, Weller M, Fisher B, Taphoorn MJ, et al. Radiotherapy plus concomitant and adjuvant temozolomide for glioblastoma. The New England journal of medicine 2005;352:987–96 [PubMed: 15758009]

3. Barbagallo GM, Jenkinson MD, Brodbelt AR. 'Recurrent' glioblastoma multiforme, when should we reoperate? Br J Neurosurg 2008;22:452–5 [PubMed: 18568742]

4. Scoccianti S, Perna M, Olmetto E, Delli Paoli C, Terziani F, Ciccone LP, et al. Local treatment for relapsing glioblastoma: A decision-making tree for choosing between reirradiation and second surgery. Crit Rev Oncol Hematol 2021;157:103184 [PubMed: 33307416]

5. Wernicke AG, Smith AW, Taube S, Mehta MP. Glioblastoma: Radiation treatment margins, how small is large enough? Pract Radiat Oncol 2016;6:298–305 [PubMed: 26952812]

6. Wang J, Cazzato E, Ladewig E, Frattini V, Rosenbloom DI, Zairis S, et al. Clonal evolution of glioblastoma under therapy. Nat Genet 2016;48:768–76 [PubMed: 27270107]

7. van Deursen JM. The role of senescent cells in ageing. Nature 2014;509:439–46 [PubMed: 24848057]

8. Wang B, Kohli J, Demaria M. Senescent Cells in Cancer Therapy: Friends or Foes? Trends Cancer 2020

9. Coppe JP, Desprez PY, Krtolica A, Campisi J. The senescence-associated secretory phenotype: the dark side of tumor suppression. Annu Rev Pathol 2010;5:99–118 [PubMed: 20078217]

10. Demaria M, O'Leary MN, Chang J, Shao L, Liu S, Alimirah F, et al. Cellular Senescence Promotes Adverse Effects of Chemotherapy and Cancer Relapse. Cancer discovery 2017;7:165–76 [PubMed: 27979832]

11. Coppe JP, Kauser K, Campisi J, Beausejour CM. Secretion of vascular endothelial growth factor by primary human fibroblasts at senescence. J Biol Chem 2006;281:29568–74 [PubMed: 16880208]

12. Parrinello S, Coppe JP, Krtolica A, Campisi J. Stromal-epithelial interactions in aging and cancer: senescent fibroblasts alter epithelial cell differentiation. J Cell Sci 2005;118:485–96 [PubMed: 15657080]

13. Liu D, Hornsby PJ. Senescent human fibroblasts increase the early growth of xenograft tumors via matrix metalloproteinase secretion. Cancer research 2007;67:3117–26 [PubMed: 17409418]

14. Tsai KK, Chuang EY, Little JB, Yuan ZM. Cellular mechanisms for low-dose ionizing radiation-induced perturbation of the breast tissue microenvironment. Cancer research 2005;65:6734–44 [PubMed: 16061655]

15. Coppe JP, Patil CK, Rodier F, Sun Y, Munoz DP, Goldstein J, et al. Senescence-associated secretory phenotypes reveal cell-nonautonomous functions of oncogenic RAS and the p53 tumor suppressor. PLoS Biol 2008;6:2853–68 [PubMed: 19053174]

16. Krtolica A, Parrinello S, Lockett S, Desprez PY, Campisi J. Senescent fibroblasts promote epithelial cell growth and tumorigenesis: a link between cancer and aging. Proc Natl Acad Sci U S A 2001;98:12072–7 [PubMed: 11593017]

17. Ruhland MK, Loza AJ, Capietto AH, Luo X, Knolhoff BL, Flanagan KC, et al. Stromal senescence establishes an immunosuppressive microenvironment that drives tumorigenesis. Nature communications 2016;7:11762

18. Bavik C, Coleman I, Dean JP, Knudsen B, Plymate S, Nelson PS. The gene expression program of prostate fibroblast senescence modulates neoplastic epithelial cell proliferation through paracrine mechanisms. Cancer research 2006;66:794–802 [PubMed: 16424011]

19. Yoshimoto S, Loo TM, Atarashi K, Kanda H, Sato S, Oyadomari S, et al. Obesity-induced gut microbial metabolite promotes liver cancer through senescence secretome. Nature 2013;499:97–101 [PubMed: 23803760]

20. Turnquist C, Beck JA, Horikawa I, Obiorah IE, Von Muhlinen N, Vojtesek B, et al. Radiation-induced astrocyte senescence is rescued by Delta133p53. Neuro Oncol 2019;21:474–85 [PubMed: 30615147]

21. Yabluchanskiy A, Tarantini S, Balasubramanian P, Kiss T, Csipo T, Fulop GA, et al. Pharmacological or genetic depletion of senescent astrocytes prevents whole brain irradiation-induced impairment of neurovascular coupling responses protecting cognitive function in mice. Geroscience 2020;42:409–28 [PubMed: 31960269]

22. Chinta SJ, Woods G, Demaria M, Rane A, Zou Y, McQuade A, et al. Cellular Senescence Is Induced by the Environmental Neurotoxin Paraquat and Contributes to Neuropathology Linked to Parkinson's Disease. Cell Rep 2018;22:930–40 [PubMed: 29386135]

23. Bhat R, Crowe EP, Bitto A, Moh M, Katsetos CD, Garcia FU, et al. Astrocyte senescence as a component of Alzheimer's disease. PLoS One 2012;7:e45069 [PubMed: 22984612]

24. Turnquist C, Horikawa I, Foran E, Major EO, Vojtesek B, Lane DP, et al. p53 isoforms regulate astrocyte-mediated neuroprotection and neurodegeneration. Cell Death Differ 2016;23:1515–28 [PubMed: 27104929]

25. Jurk D, Wang C, Miwa S, Maddick M, Korolchuk V, Tsolou A, et al. Postmitotic neurons develop a p21-dependent senescence-like phenotype driven by a DNA damage response. Aging Cell 2012;11:996–1004 [PubMed: 22882466]

26. Bussian TJ, Aziz A, Meyer CF, Swenson BL, van Deursen JM, Baker DJ. Clearance of senescent glial cells prevents tau-dependent pathology and cognitive decline. Nature 2018;562:578–82 [PubMed: 30232451]

27. Robbins PD, Jurk D, Khosla S, Kirkland JL, LeBrasseur NK, Miller JD, et al. Senolytic Drugs: Reducing Senescent Cell Viability to Extend Health Span. Annu Rev Pharmacol Toxicol 2021;61:779–803 [PubMed: 32997601]

28. Kirkland JL, Tchkonia T. Senolytic drugs: from discovery to translation. J Intern Med 2020;288:518–36 [PubMed: 32686219]

29. Deng C, Zhang P, Harper JW, Elledge SJ, Leder P. Mice lacking p21CIP1/WAF1 undergo normal development, but are defective in G1 checkpoint control. Cell 1995;82:675–84 [PubMed: 7664346]

30. Todorova PK, Fletcher-Sananikone E, Mukherjee B, Kollipara R, Vemireddy V, Xie XJ, et al. Radiation-Induced DNA Damage Cooperates with Heterozygosity of TP53 and PTEN to Generate High-Grade Gliomas. Cancer research 2019;79:3749–61 [PubMed: 31088835]

31. Mangoni M, Sottili M, Gerini C, Desideri I, Bastida C, Pallotta S, et al. A PPAR gamma agonist protects against oral mucositis induced by irradiation in a murine model. Oral Oncol 2017;64:52–8 [PubMed: 28024724]

32. Oh T, Fakurnejad S, Sayegh ET, Clark AJ, Ivan ME, Sun MZ, et al. Immunocompetent murine models for the study of glioblastoma immunotherapy. J Transl Med 2014;12:107 [PubMed: 24779345]

33. Gil del Alcazar CR, Hardebeck MC, Mukherjee B, Tomimatsu N, Gao X, Yan J, et al. Inhibition of DNA double-strand break repair by the dual PI3K/mTOR inhibitor NVP-BEZ235 as a strategy for radiosensitization of glioblastoma. Clin Cancer Res 2014;20:1235–48 [PubMed: 24366691]

34. Sennino B, Ishiguro-Oonuma T, Wei Y, Naylor RM, Williamson CW, Bhagwandin V, et al. Suppression of tumor invasion and metastasis by concurrent inhibition of c-Met and VEGF signaling in pancreatic neuroendocrine tumors. Cancer discovery 2012;2:270–87 [PubMed: 22585997]

35. Schildge S, Bohrer C, Beck K, Schachtrup C. Isolation and culture of mouse cortical astrocytes. Journal of visualized experiments : JoVE 2013

36. Trapnell C, Pachter L, Salzberg SL. TopHat: discovering splice junctions with RNA-Seq. Bioinformatics 2009;25:1105–11 [PubMed: 19289445]

37. Trapnell C, Roberts A, Goff L, Pertea G, Kim D, Kelley DR, et al. Differential gene and transcript expression analysis of RNA-seq experiments with TopHat and Cufflinks. Nat Protoc 2012;7:562–78 [PubMed: 22383036]

38. Dimri GP, Lee X, Basile G, Acosta M, Scott G, Roskelley C, et al. A biomarker that identifies senescent human cells in culture and in aging skin in vivo. Proc Natl Acad Sci U S A 1995;92:9363–7 [PubMed: 7568133]

39. von Bartheld CS, Bahney J, Herculano-Houzel S. The search for true numbers of neurons and glial cells in the human brain: A review of 150 years of cell counting. J Comp Neurol 2016;524:3865–95 [PubMed: 27187682]

40. Sofroniew MV, Vinters HV. Astrocytes: biology and pathology. Acta Neuropathol 2010;119:7–35 [PubMed: 20012068]

41. Freund A, Laberge RM, Demaria M, Campisi J. Lamin B1 loss is a senescence-associated biomarker. Molecular biology of the cell 2012;23:2066–75 [PubMed: 22496421]

42. Gorgoulis V, Adams PD, Alimonti A, Bennett DC, Bischof O, Bishop C, et al. Cellular Senescence: Defining a Path Forward. Cell 2019;179:813–27 [PubMed: 31675495]

43. Lopes-Paciencia S, Saint-Germain E, Rowell MC, Ruiz AF, Kalegari P, Ferbeyre G. The senescence-associated secretory phenotype and its regulation. Cytokine 2019;117:15–22 [PubMed: 30776684]

44. Cerami E, Gao J, Dogrusoz U, Gross BE, Sumer SO, Aksoy BA, et al. The cBio cancer genomics portal: an open platform for exploring multidimensional cancer genomics data. Cancer discovery 2012;2:401–4 [PubMed: 22588877]

45. Gao J, Aksoy BA, Dogrusoz U, Dresdner G, Gross B, Sumer SO, et al. Integrative analysis of complex cancer genomics and clinical profiles using the cBioPortal. Science signaling 2013;6:pl1

46. Owusu BY, Galemmo R, Janetka J, Klampfer L. Hepatocyte Growth Factor, a Key Tumor-Promoting Factor in the Tumor Microenvironment. Cancers 2017;9

47. Boccaccio C, Comoglio PM. MET, a driver of invasive growth and cancer clonal evolution under therapeutic pressure. Curr Opin Cell Biol 2014;31:98–105 [PubMed: 25305631]

48. Camacho CV, Todorova PK, Hardebeck MC, Tomimatsu N, Gil del Alcazar CR, Ilcheva M, et al. DNA double-strand breaks cooperate with loss of Ink4 and Arf tumor suppressors to generate glioblastomas with frequent Met amplification. Oncogene 2015;34:1064–72 [PubMed: 24632607]

49. Cruickshanks N, Zhang Y, Yuan F, Pahuski M, Gibert M, Abounader R. Role and Therapeutic Targeting of the HGF/MET Pathway in Glioblastoma. Cancers 2017;9

50. Karpel-Massler G, Ishida CT, Bianchetti E, Zhang Y, Shu C, Tsujiuchi T, et al. Induction of synthetic lethality in IDH1-mutated gliomas through inhibition of Bcl-xL. Nature communications 2017;8:1067

51. Gupta K, Vuckovic I, Zhang S, Xiong Y, Carlson BL, Jacobs J, et al. Radiation Induced Metabolic Alterations Associate With Tumor Aggressiveness and Poor Outcome in Glioblastoma. Front Oncol 2020;10:535 [PubMed: 32432031]

52. Abounader R, Laterra J. Scatter factor/hepatocyte growth factor in brain tumor growth and angiogenesis. Neuro Oncol 2005;7:436–51 [PubMed: 16212809]

53. Straussman R, Morikawa T, Shee K, Barzily-Rokni M, Qian ZR, Du J, et al. Tumour micro-environment elicits innate resistance to RAF inhibitors through HGF secretion. Nature 2012;487:500–4 [PubMed: 22763439]

54. Nakamura T, Matsumoto K, Kiritoshi A, Tano Y, Nakamura T. Induction of hepatocyte growth factor in fibroblasts by tumor-derived factors affects invasive growth of tumor cells: in vitro analysis of tumor-stromal interactions. Cancer research 1997;57:3305–13 [PubMed: 9242465]

55. Zhu Y, Tchkonia T, Fuhrmann-Stroissnigg H, Dai HM, Ling YY, Stout MB, et al. Identification of a novel senolytic agent, navitoclax, targeting the Bcl-2 family of anti-apoptotic factors. Aging Cell 2016;15:428–35 [PubMed: 26711051]

56. Chang J, Wang Y, Shao L, Laberge RM, Demaria M, Campisi J, et al. Clearance of senescent cells by ABT263 rejuvenates aged hematopoietic stem cells in mice. Nat Med 2016;22:78–83 [PubMed: 26657143]

57. Jeon OH, Kim C, Laberge RM, Demaria M, Rathod S, Vasserot AP, et al. Local clearance of senescent cells attenuates the development of post-traumatic osteoarthritis and creates a pro-regenerative environment. Nat Med 2017;23:775–81 [PubMed: 28436958]

58. Pan J, Li D, Xu Y, Zhang J, Wang Y, Chen M, et al. Inhibition of Bcl-2/xl With ABT-263 Selectively Kills Senescent Type II Pneumocytes and Reverses Persistent Pulmonary Fibrosis Induced by Ionizing Radiation in Mice. International journal of radiation oncology, biology, physics 2017;99:353–61 [PubMed: 28479002]

59. Lagares D, Santos A, Grasberger PE, Liu F, Probst CK, Rahimi RA, et al. Targeted apoptosis of myofibroblasts with the BH3 mimetic ABT-263 reverses established fibrosis. Sci Transl Med 2017;9

60. Khan S, Zhang X, Lv D, Zhang Q, He Y, Zhang P, et al. A selective BCL-XL PROTAC degrader achieves safe and potent antitumor activity. Nat Med 2019;25:1938–47 [PubMed: 31792461]

61. Prasanna PG, Citrin DE, Hildesheim J, Ahmed MM, Venkatachalam S, Riscuta G, et al. Therapy-Induced Senescence: Opportunities to Improve Anti-Cancer Therapy. J Natl Cancer Inst 2021

62. Aasland D, Gotzinger L, Hauck L, Berte N, Meyer J, Effenberger M, et al. Temozolomide Induces Senescence and Repression of DNA Repair Pathways in Glioblastoma Cells via Activation of ATR-CHK1, p21, and NF-kappaB. Cancer research 2019;79:99–113 [PubMed: 30361254]

63. Zhang L, Cheng F, Wei Y, Zhang L, Guo D, Wang B, et al. Inhibition of TAZ contributes radiation-induced senescence and growth arrest in glioma cells. Oncogene 2019;38:2788–99 [PubMed: 30542117]

64. Milanovic M, Fan DNY, Belenki D, Dabritz JHM, Zhao Z, Yu Y, et al. Senescence-associated reprogramming promotes cancer stemness. Nature 2018;553:96–100 [PubMed: 29258294]

65. Wissler Gerdes EO, Zhu Y, Weigand BM, Tripathi U, Burns TC, Tchkonia T, et al. Cellular senescence in aging and age-related diseases: Implications for neurodegenerative diseases. Int Rev Neurobiol 2020;155:203–34 [PubMed: 32854855]
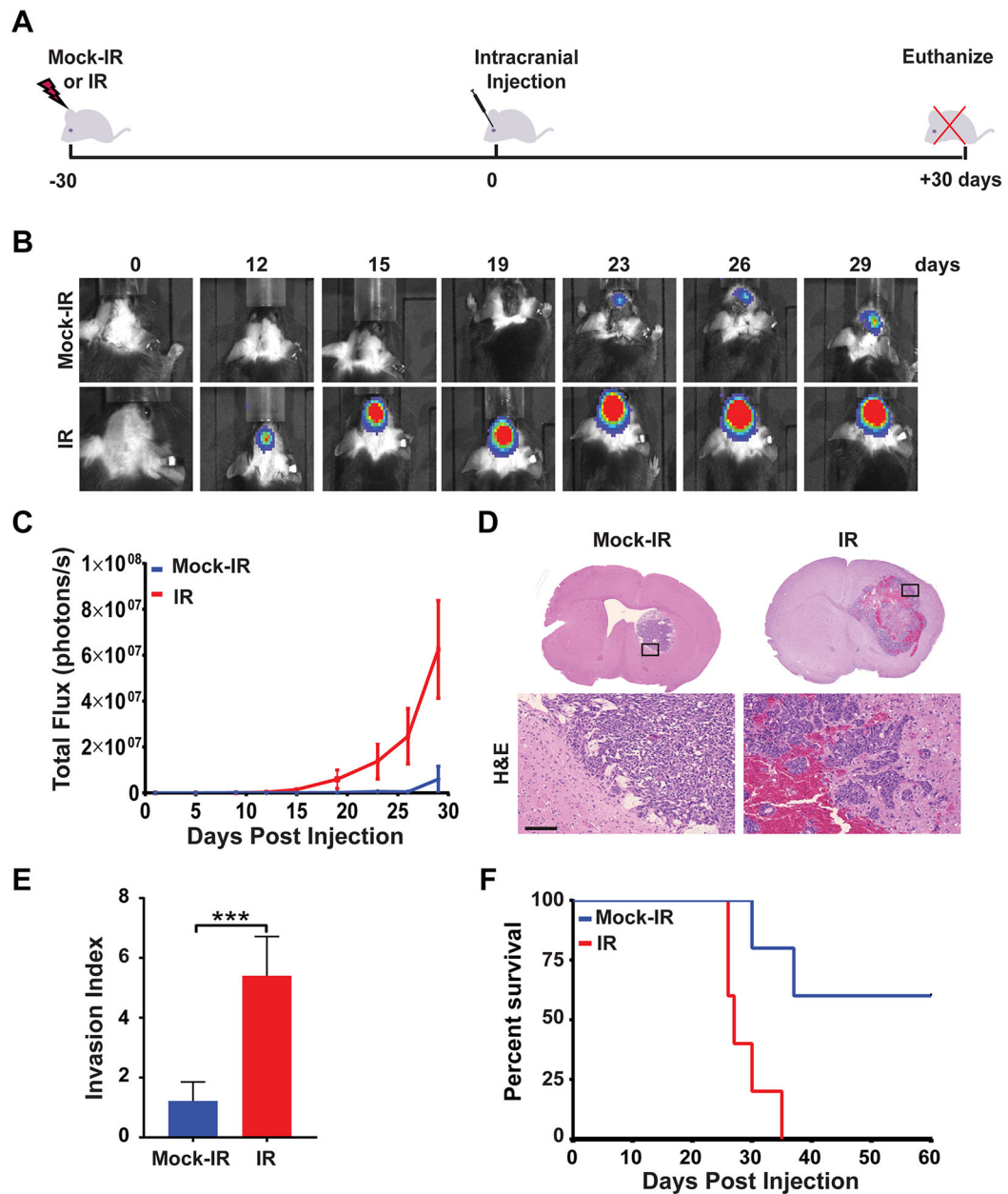
Statement of Significance

This study uncovers mechanisms by which radiation can promote GBM recurrence by inducing senescence in non-neoplastic brain cells, suggesting that senolytic therapy can blunt recurrent GBM growth and aggressiveness.

Figure 1. Irradiation of the brain promotes GBM growth and aggressiveness.
A, Schematic of experimental design. **B,** C57BL/6J mice were mock irradiated (Mock-IR) or cranially irradiated (IR) with 10 Gy of X-rays (6 mice per cohort). After 30 days, mice were intra-cranially implanted with 2,500 GL261 cells expressing firefly luciferase. Tumor growth was monitored by BLI imaging over a 30-day period. BLI images show tumor progression in a representative mouse for each cohort. **C,** Plot represents average signal intensity (photons per second) for each cohort versus time post-injection. Note marked increase in the rate of tumor growth (*red line*) in pre-irradiated mouse brains (P=0.0278, error bars S.E.M). **D,** H&E-stained sections of mock-irradiated or irradiated mouse brains bearing GL261 tumors. High magnifications show representative areas spanning the tumor borders. Note marked increase in tumor size and infiltration in the pre-irradiated mouse
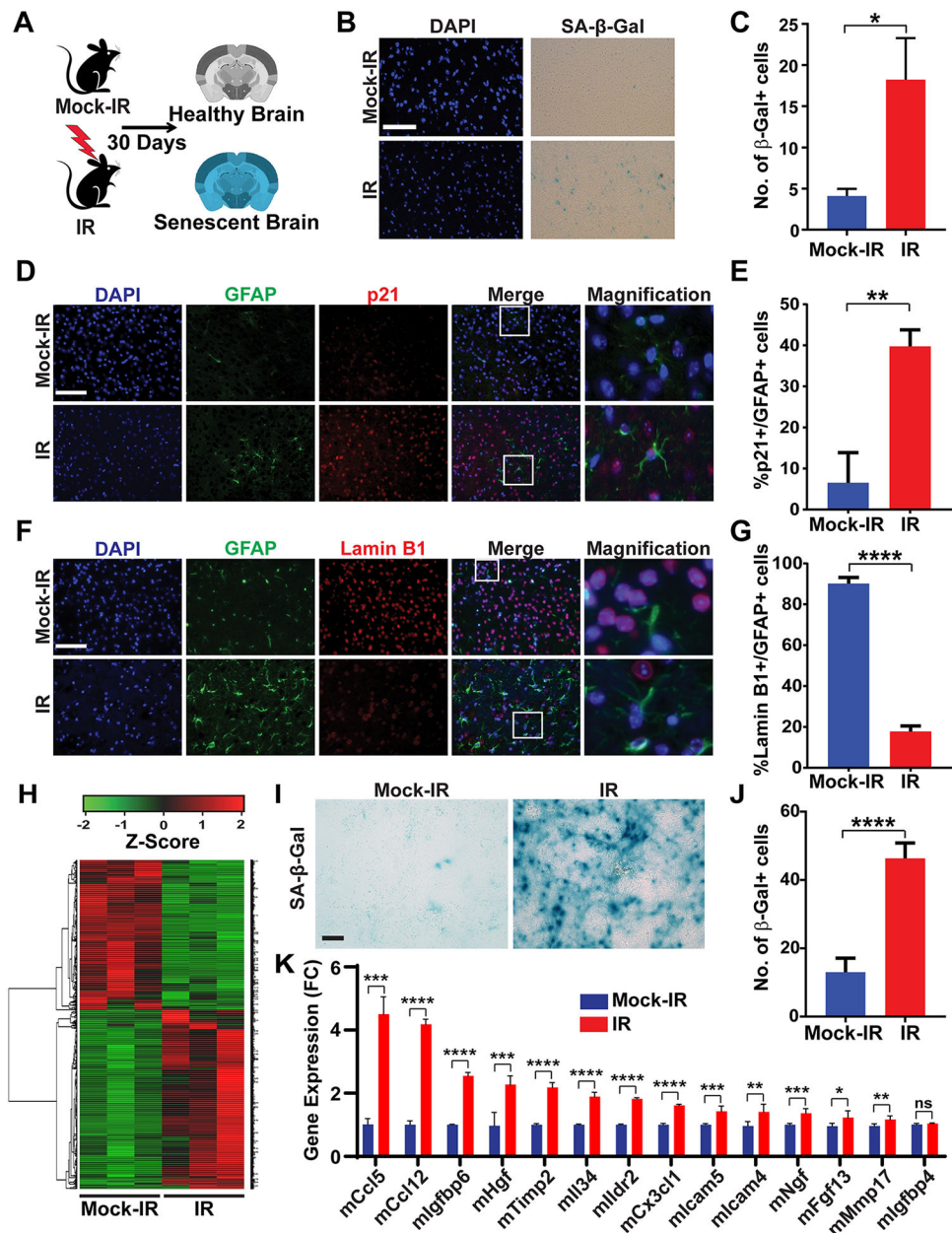
brain. Scale bar=100 μm. **E,** Plot depicts average Invasion Index for mock-irradiated or irradiated cohorts (P= 0.0002, error bars S.D). **F,** Kaplan-Meier curves show survival of mock-irradiated or pre-irradiated mice implanted with GL261 cells and then monitored over a 60-day period (n=6 per cohort, P=0.0086).

**Figure 2. Ionizing radiation triggers senescence and the SASP in the brain.**
A, Schematic of experimental design. **B,** Mice were mock-irradiated or irradiated with 10 Gy of X-rays and then allowed to recover for 30 days (3 mice per cohort). Senescence was measured at 30 days post-irradiation by staining brain sections for SA-β-Gal activity. Representative Images of SA-β-Gal and DAPI (blue) staining of the cortex of brains of mock-irradiated and irradiated mice are shown. Scale bar=100 μm. **C,** Plot shows numbers of SA-β-Gal cells per 40X microscopic field in brains of mock-irradiated and irradiated mice (n=3 for each cohort, P=0.0372, error bars S.D). **D,** Images show immunofluorescence staining of the cortex of mock-irradiated and irradiated brains for GFAP (green), p21 (red) and DAPI (blue). Scale bar=50 μm. **E,** Plot shows the percentage of GFAP-positive cells that stain positive for p21 in mock-irradiated and irradiated brains (n=3 per cohort,

P=0.0058, error bars S.D). **F,** Images show immunofluorescence staining of the cortex of mock-irradiated and irradiated brains for GFAP (green), Lamin B1 (red) and DAPI (blue). Scale bar=50 μm. **G,** Plot shows the percentage of GFAP-positive cells that stain positive for Lamin B1 in mock-irradiated and irradiated brains (n=3 per cohort, P <0.0001, error bars S.D). Note that irradiated brains exhibit positivity for multiple markers of senescence. **H,** Heatmap of differentially expressed genes in brain tissues from mice that were mock-irradiated or irradiated with 10 Gy of X-rays and then allowed to recover for 30 days (3 mice per cohort). **I,** Representative image of SA-β-Gal staining of primary mouse astrocytes mock-irradiated or irradiated with 10 Gy of X-rays and then allowed to recover for 10 days. Scale bar=100 μm. **J,** Plot shows number of SA-β-Gal-positive cells per 40X microscopic field (n=3, P<0.0001, error bars S.D). **K,** Plot shows relative expression of SASP-related genes in mock-irradiated versus irradiated astrocytes as quantified by qRT-PCR. (n=3; *, P 0.05; **, P 0.01; ***, P 0.001 ****, P 0.0001; error bars S.D).
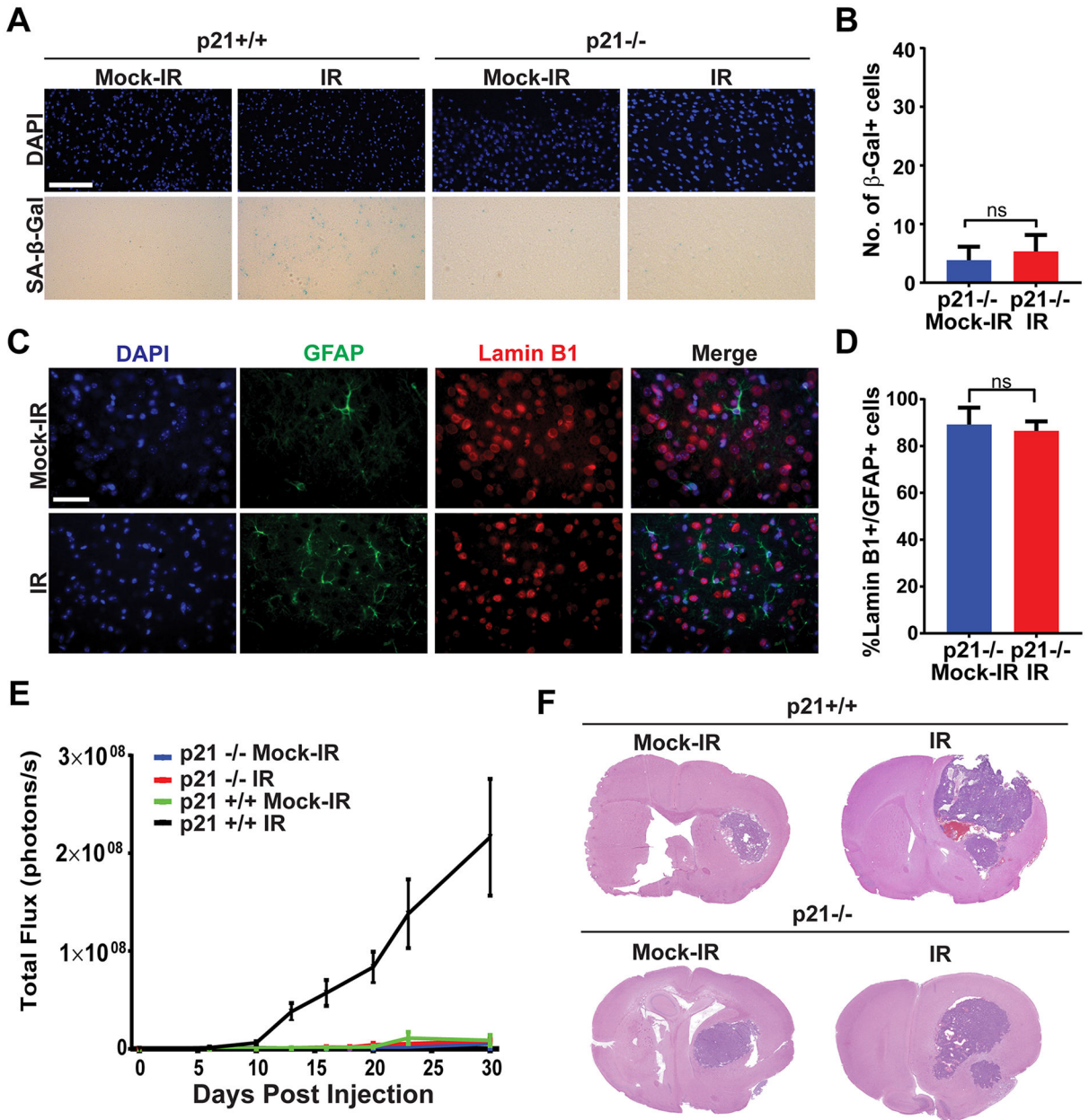
Figure 3. Senescence induction and tumor promotion by ionizing radiation are p21-dependent.
A, p21+/+ or p21−/− mice were mock-irradiated or irradiated with 10 Gy of X-rays and then allowed to recover for 30 days (6 mice per cohort). Senescence was measured at 30 days post-IR by staining brain sections for SA-β-Gal activity. Representative Images of SA-β-Gal and DAPI (blue) staining of the cortex of brains of mock-irradiated and irradiated mice are shown. Scale bar=100 μm. **B,** Plot shows numbers of SA-β-Gal cells per 40X microscopic field in brains of mock-irradiated and irradiated mice (n=6 for each cohort, P=0.3371, error bars S.D). **C,** Images show immunofluorescence staining of the cortex of mock-irradiated and irradiated p21−/− brains for GFAP (green), Lamin B1 (red) and DAPI (blue). Scale bar=50 μm. **D,** Plot shows the percentage of GFAP-positive cells that stain positive for Lamin B1 in mock-irradiated and irradiated brains (n=3 per cohort, P= 0.6117,

error bars S.D). Note that irradiated p21−/− brains do not stain for senescence markers. **E,** p21+/+ or p21−/− mice were mock irradiated or cranially irradiated with 10 Gy of X-rays (6 mice per cohort). After 30 days, mice were intra-cranially implanted with 2,500 GL261 cells expressing firefly luciferase. Tumor growth was monitored by BLI imaging. Plot represents average signal intensity (photons per second) for each cohort versus time post-injection. Note promotion of tumor growth in irradiated p21+/+ mice but not in p21−/− mice (p21−/− IR vs p21+/+ IR P= 0.0082, p21−/− Mock vs p21−/− IR P=0.6448, error bars S.E.M). **F,** H&E-stained sections of mock-irradiated or irradiated p21+/+ and p21−/− mouse brains bearing GL261 tumors.
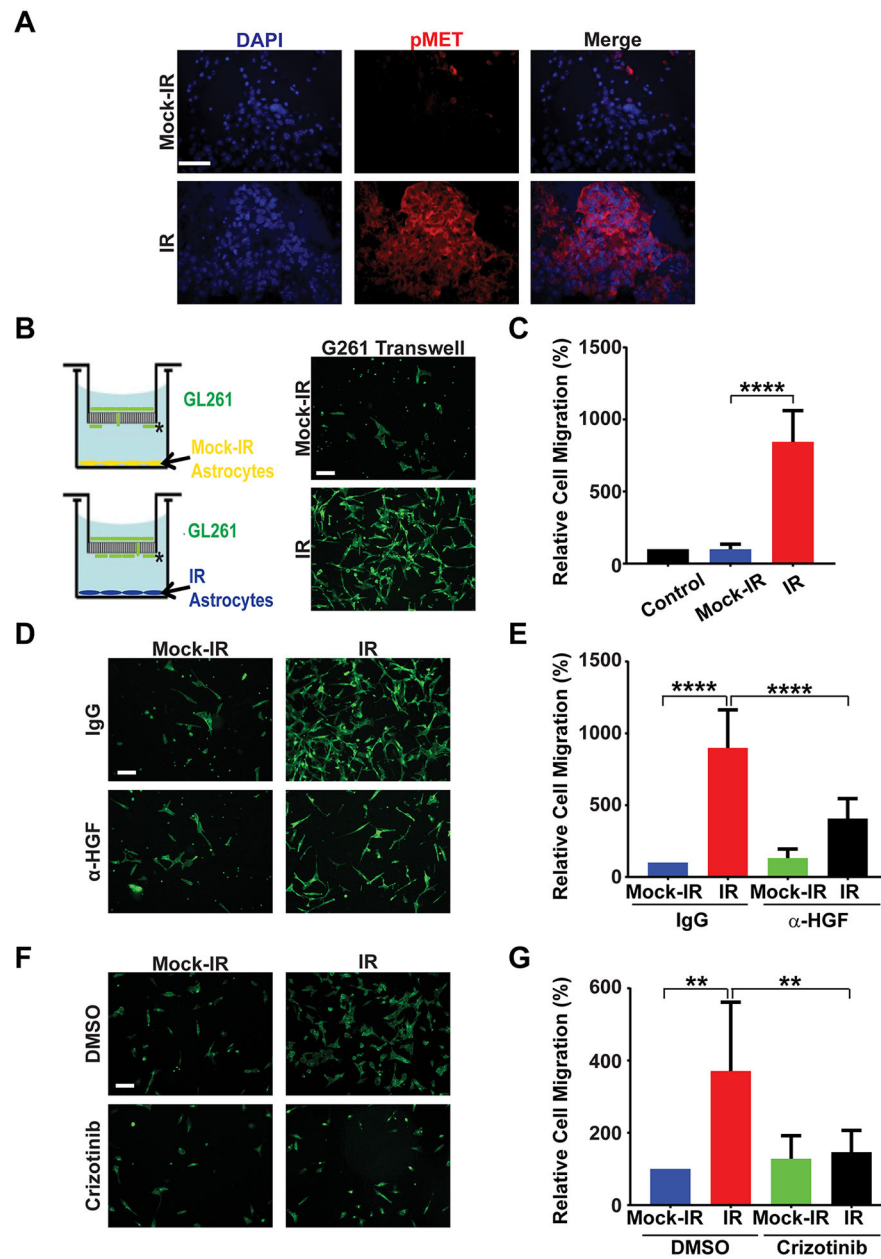
Figure 4. Senescent astrocytes promote migration of GBM cells in vitro.
A, GL261 tumors growing in mock-irradiated or pre-irradiated (10 Gy, 30 days) brains were sectioned and stained for phospho-Met (Y1234/1235; red) and DAPI (blue). Representative images are shown (n=3 per cohort). Note robust Met activation in tumor growing in pre-irradiated brain. Scale bar=50 μm. **B,** Schematic of Boyden Chamber Assay with GL261 cells in the top chamber and mock-irradiated or irradiated (10 Gy, 10 days) primary mouse astrocytes in the bottom chamber. Representative images of GL261 cells on the bottom surface of the trans-well membrane (indicated by *) stained with Alexa Fluor 488 Phalloidin (green). Scale bar=100 μm. **C,** Plot shows percentage of cells per 40X microscopic field migrating towards the bottom chamber relative to migration towards media alone (n=3, P<0.0001, error bars S.D). Control represents assay with only cell culture media in the

bottom chamber (no astrocytes). **D,** Representative fluorescence images of GL261 cells treated with either IgG or α-HGF antibody in a Boyden Chamber migration assay with mock-irradiated or irradiated primary astrocytes in the bottom chamber. Scale bar=100 μM. **E,** Plot shows percentage of cells per 40X microscopic field migrating towards the bottom chamber relative to migration towards IgG-treated mock-irradiated astrocytes (n=3, IR/IgG vs IR/αHGF P<0.0001, error bars S.D). **F,** Representative fluorescence images of GL261 cells treated with either DMSO or Crizotnib in a Boyden Chamber migration assay with mock-irradiated or irradiated primary astrocytes in the bottom chamber. Scale bar=100 μm. **G,** Plot shows percentage of cells per 40X microscopic field migrating towards the bottom chamber relative to migration towards DMSO-treated mock-irradiated astrocytes (n=3, IR/ DMSO vs IR/Crizotinib P=0.0047, error bars S.D).
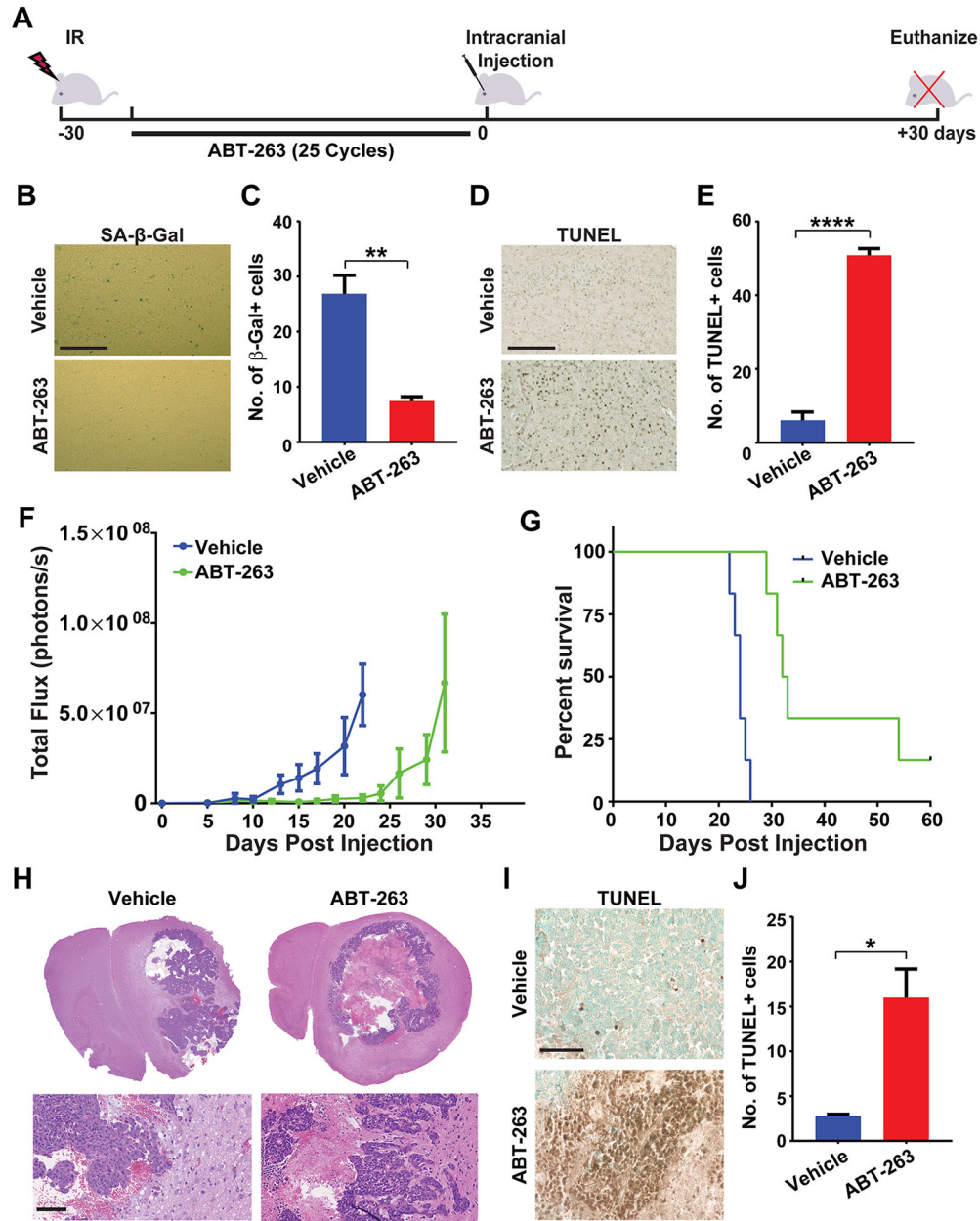
Figure 5. ABT-263 eliminates senescent cells in vivo and attenuates GBM growth.
A, Schematic of experimental design. **B,** C57BL/6J mice were cranially irradiated with 10 Gy of X-rays (3 mice per cohort). After 5 days, mice were treated with either vehicle or ABT-263 (50 mg/kg) daily for 25 days. Senescence was measured at 30 days post-IR by staining brain sections for SA-β-Gal activity. Representative Images of SA-β-Gal staining of the cortex of brains of cranially irradiated mice treated with vehicle or ABT-263 are shown. Scale bar=100 μm. **C,** Plot shows numbers of SA-β-Gal cells per 40X microscopic field in brains of vehicle or ABT-263 treated mice (n=3 for each cohort, P= 0.0072, error bars S.D). **D,** Representative Images of TUNEL staining of the cortex of brains of cranially irradiated mice treated with vehicle or ABT-263 are shown. Scale bar=100 μm. **E,** Plot shows number of TUNEL-positive cells per 40X microscopic field in brains of vehicle- or

ABT-263-treated mice (n=3 for each cohort, P<0.0001, error bars S.D). **F,** C57BL/6J mice were mock irradiated or cranially irradiated with 10 Gy of X-rays (6 mice per cohort). After 5 days, mice were treated with either vehicle or ABT-263 (50 mg/kg) daily for 25 days. At 30 days post-IR, mice were intra-cranially implanted with 2,500 GL261 cells expressing firefly luciferase. Tumor growth was monitored by BLI imaging over a 30-day period. Plot represents average signal intensity (photons per second) for each cohort versus time post-injection. (P=0.0074, error bars S.E.M). Note marked delay in tumor growth (*green line*) in mouse brains pre-treated with ABT-263. **G,** Kaplan-Meier curves show survival of pre-irradiated mice, treated with vehicle or ABT-263, implanted with GL261 cells and then monitored over a 60-day period. (n=6 per cohort, P=0.0005). **H,** H&E-stained sections of GL261 tumors in pre-irradiated mouse brains treated with vehicle or ABT-263 prior to tumor cell implantation. Note: tumors in ABT-263-treated mice are highly necrotic with undefined borders. Scale bar =100 μM. **I,** Representative TUNEL images of GL261 tumors in vehicle or ABT-263 treated irradiated mouse brains. Scale bar=100 μm. **J,** Plot shows number of TUNEL-positive cells per 40X microscopic field in GL261 tumors in vehicle or ABT-263 treated mice (n=3 for each cohort, P=0.0184, error bars S.D).